Unusual electronic state of Sn in $AgSnSe_2$

Y. Naijo,[1] K. Hada,[1] T. Furukawa,[1,*] T. Itou,[1] T. Ueno,[2] K. Kobayashi,[2] I. I. Mazin,[3,†] H. O. Jeschke,[2] and J. Akimitsu[2]
[1]Department of Applied Physics, Tokyo University of Science, Tokyo 125-8585, Japan
[2]Research Institute for Interdisciplinary Science, Okayama University, Okayama 700-8530, Japan
[3]Naval Research Laboratory, Washington, DC 20375, USA

(Received 22 September 2019; revised manuscript received 5 February 2020; accepted 5 February 2020; published 25 February 2020)

$AgSnSe_2$, by formal electron count, should have Sn in a highly unusual 3+ valence state and was therefore suggested to be a valence-skipping compound with potential for negative-U centers and local electron pairing. It has been proposed that the latter may be the mechanism beyond seemingly conventional superconductivity in this compound. We report NMR measurements and first-principles calculations that agree with each other perfectly, and both indicate that valence skipping does not take place and the highly unusual Sn^{3+} state is realized instead, likely because of geometrical constraint prohibiting a breathing distortion that could screen the on-site Coulomb repulsion.

DOI: 10.1103/PhysRevB.101.075134

I. BACKGROUND

An interesting and not fully understood phenomenon called "valence skipping" occurs for particular elements in most solid compounds [1]. Typical examples are Sn and Pb with their valence states +2 and +4, but not +3, and Bi and Sb, with +3 and +5, but not +4. Whatever the microscopic origin of valence skipping is, it may be phenomenologically described in terms of "negative U centers," i.e., as an on-site attraction between electrons. On a model level, such an interaction leads to superconductivity [2–4]. Not surprisingly, it was suggested to play a role in superconductivity in several valence-skipping materials, such as $(Ba,K)BiO_3$ [1,5–8] (perovskite structure) or (Pb,Tl)Te [9–13] (NaCl-type structure). Still, in spite of a considerable effort, no conclusive experimental proof has been presented so far.

Typically, if the nominal valence is a skipped one, the material experiences charge disproportionation, for instance, into Sn^{2+} and Sn^{4+}. Since regular on-site Coulomb repulsion is still present, such charge transfer is always accompanied by a screening breathing distortion of anions. It is the latter that effectively enables charge disproportionation [14]. Such screening is very efficient; for instance, in $BaBiO_3$ the charge from O tails inside the Bi^{5+} atomic sphere nearly compensates the additional charge of Bi electrons [15]. Obviously, in order for a "negative-U" interaction to generate superconductivity, a local electron pair must be mobile, and with it the local breathing distortion, which is not always possible (a similar problem arises in bipolaronic theories of superconductivity).

$AgSnSe_2$ is exceptionally interesting in this aspect. It crystallizes in a simple NaCl-type structure, where Ag and Sn randomly occupy one position and Se the other. As opposed to the perovskite structure of $BaBiO_3$, this geometry does not allow for a straightforward breathing distortion, which hinders charge disproportionation. It is worth noting that despite Sn^{3+} being extremely rare, it was argued to exist in some compounds (for instance, SnP_3 [16]).

Recently Wakita *et al.* have carried out x-ray absorption spectroscopy (XAS) and x-ray photoemission spectroscopy (XPS) measurements on $AgSnSe_2$ and suggested that Sn disproportionates into Sn^{2+} and Sn^{4+} dynamically even at room temperature [17], and suggested that it may create dynamic negative-U centers and facilitate superconductivity there. Nasredinov *et al.* reported that the Sn Mössbauer spectra of $AgSnSe_2$ represent single lines [18], which can be interpreted either as the dynamical disproportionation on a scale faster than the Mössbauer timescale or as undisproportionated Sn^{3+} without valence skipping. In this article, we address this issue using first-principles calculations, Sn- and Se-NMR spectroscopy, and spin-lattice relaxation measurements. We find both the theoretical and experimental results to be in excellent agreement with each other, and both show undisproportionated Sn^{3+}.

II. EXPERIMENTAL METHODS

Polycrystalline $Ag_{1-x}Sn_{1+x}Se_2$ crystals were synthesized by a conventional melt growth method. The compound studied here is $Ag_{0.8}Sn_{1.2}Se_2$, where the highest T_c has been observed [19,20]. The stoichiometric ratios of Ag, Sn, and Se powder were weighed and pelletized before being sealed in a quartz tube. They are heated at 800 °C for 2 days and cooled down to room temperature for 5 h. The obtained crystals were grounded and pelletized again before sealing them in an evacuated quartz tube. They are heated at 500 °C for 2 days before being quenched in water. The obtained crystals have a silver metallic surface. They were ground into grains

*Present address: Institute for Materials Research, Tohoku University, Sendai 980-8577, Japan.
†Present address: Department of Physics and Astronomy, George Mason University, Fairfax, VA 22030, USA.

of 100–700 μm in size to prevent the reduction of the NMR signal by the radio-frequency skin effect.

The field-sweep NMR measurements were carried out at 3.62 and 1.93 K on ^{119}Sn nuclei (nuclear spin $I = 1/2$ and $\gamma = 15.867$ MHz/T) and ^{117}Sn nuclei (nuclear spin $I = 1/2$ and $\gamma = 15.168$ MHz/T) at a fixed frequency of 133.35 MHz, which corresponds to resonance fields of 8.404 T for ^{119}Sn and 8.792 T for ^{117}Sn. The NMR signal intensities were obtained by integration of the spin-echo signals following a $\pi/2 - \tau - \pi$ pulse sequence. The widths of the $\pi/2$ and π pulses were typically 3.5 and 7 μs, respectively, and τ was 17.5 μs. Since ^{119}Sn and ^{117}Sn have a natural abundance of only 8.6% and 7.6%, we averaged NMR signals numerous times up to 18 000. The interval delay separating two spin-echo sequences is 25 ms; as an exception, in the measurement at 3.62 K, an interval delay of 2.3 s was applied only from 8.38 to 8.42 T, because a long-interval measurement is needed to observe the NMR signals at around 8.4 T owing to a long spin-lattice relaxation time.

The NMR spectra of ^{77}Se ($I = 1/2$ and $\gamma = 8.13$ MHz/T) were obtained by a Fourier transformation of the spin-echo signals following a $\pi/2 - \tau - \pi$ pulse sequence under 8.7 T. The widths of the $\pi/2$ and π pulses were typically 3.8 and 7.6 μs (6 and 12 μs) in the temperature range 1.5–10 K (20–270 K), respectively. Although the frequency range to be covered by these pulses is within approximately ± 50 kHz, the observed NMR spectra are broadened beyond this range; therefore, we measured spin-echo signals at various frequencies with an interval of 10 or 20 kHz, and the entire spectra were then constructed by combining these local spectra.

We could not perform detailed measurements of the ^{119}Sn and ^{117}Sn spin-lattice relaxation rate T_1^{-1}. This was because of the broad ^{119}Sn and ^{117}Sn spectrum ($\sim$0.2 T, corresponding to $\sim$3 MHz), which causes the following two difficulties: (i) the observed NMR signal was too weak to obtain accurate spin-lattice relaxation curves, and (ii) the spin-lattice relaxation curves are seriously affected by the spin diffusion effect, making it difficult to obtain information on the intrinsic relaxation rate. As an alternative, we measured T_1^{-1} of the ^{77}Se nuclei by the standard saturation recovery method. We determined ^{77}Se T_1^{-1} by fitting the spin-echo intensity $M(t)$ after a time delay t following saturation comb pulses to a single-exponential function $1 - M(t)/M(\infty) = \exp(-t/T_1)$.

III. COMPUTATIONAL METHODS

We use density functional theory (DFT) with a projector augmented wave (PAW) basis as implemented in VASP [21] for structure optimization. In order to simulate Ag-Sn disorder we generated several randomly populated supercells with 54 formula units each, fully optimized the supercell dimensions and internal coordinates, and interrogated the system for the bond length and partial Sn-*s* densities of states. Full-scale Knight shift calculations were performed in the all-electron linearized augmented plane-wave code WIEN2K [22]. An artificial external field of 100 T was introduced, and the hyperfine fields (Fermi contact, core polarization, dipolar, and orbital) were calculated directly. In both codes the gradient-corrected density functional of Perdew *et al.* [23] was used. Convergence with respect to the plane-wave cutoffs and the *k*-point mesh density has been verified. We use the full potential local orbital [24] basis to double check the calculated charges of $AgSnSe_2$.

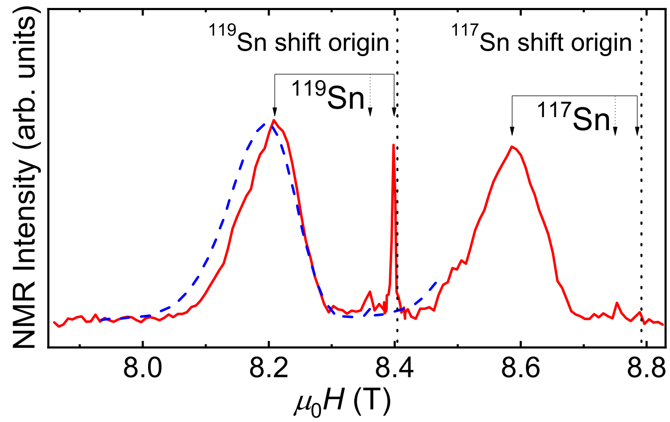

FIG. 1. Field-swept ^{119}Sn- and ^{117}Sn-NMR spectra for $AgSnSe_2$. The red solid line and blue dashed line show Sn spectrum at 3.62 and 1.93 K, respectively. The dotted straight lines indicate the shift origins for ^{119}Sn and ^{117}Sn bare nuclei.

IV. EXPERIMENTAL RESULTS

Figure 1 shows the field-swept Sn-NMR spectra measured at a fixed frequency of 133.35 MHz. The signals from 8.0 to 8.4 T and from 8.4 to 8.8 T are attributed to ^{119}Sn and ^{117}Sn nuclei, respectively. The ^{119}Sn signals observed at 3.62 K are composed of two lines—the main broad line observed from 8.1 to 8.3 T and the minor sharp line at 8.4 T. (An additional weak line may exist at 8.37 T, which is clearly an extrinsic signal because the intensity is very low.) The minor line at 8.4 T has an intensity (integration area) much smaller than that of the main broad line. Therefore, it is natural to think that the minor line is due to Sn defects and is not intrinsic for the present material. The minor line is situated near the shift origin and thus is most likely due to nonpolarizable Sn^{2+} or Sn^{4+} ions. Indeed, the spin-lattice relaxation time of the minor line at 8.4 T is long ($\sim$3.7 s at 3.62 K), which also indicates that the sites are not spin polarized. Note that a long-interval measurement is needed to observe the line with a long spin-lattice relaxation time. Such measurements were done only for the ^{119}Sn signals at 3.62 K. This is the reason why the ^{117}Sn signals at 3.62 K and the ^{119}Sn signals at 1.93 K do not show the minor line.

Except for the minor extrinsic line, the main ^{119}Sn and ^{117}Sn signals are single lines. They have a similar intensity because of the almost same natural abundances (8.6% for ^{119}Sn and 7.6% for ^{117}Sn) and the geometric ratios γ ($\gamma = 15.867$ MHz/T for ^{119}Sn, and $\gamma = 15.168$ MHz/T for ^{117}Sn). If the valence state of Sn is split into Sn^{2+} and Sn^{4+}, both ^{119}Sn and ^{117}Sn spectra should be split into double peaks corresponding to the signals from Sn^{2+} and Sn^{4+}; however, the experimental result does not show such behavior. Furthermore, the main signals have a large Knight shift (2.3%–2.4%), which indicates that Sn sites are highly polarizable. Indeed, the spin-lattice relaxation time of the main line is short (of the order of 600 μs at 3.62 K, though we could not

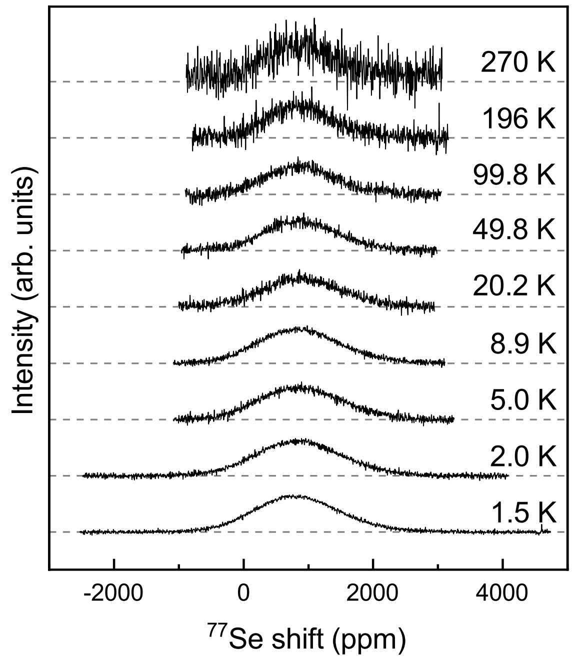

FIG. 2. Temperature dependence of the ^{77}Se NMR spectrum for $AgSnSe_2$ under 8.7 T. The origin of the horizontal axis represents the unshifted resonance frequency of ^{77}Se.

determine the value precisely because of the small intensity of the signal and the spin-diffusion effect, as explained previously). This result indicates that the sites are not Sn^{2+} or Sn^{4+}. We can thus conclude that the main spectrum is due to Sn sites whose valence is uniform and close to +3. Hence, the Sn-NMR spectral result does not indicate any sign of the static charge disproportionation due to valence skipping. Note that the linewidths of the main signals are large (of the order of 0.2 T). The reason for such large linewidths will be discussed later.

Figure 2 shows the temperature dependence of the ^{77}Se-NMR spectra obtained by the Fourier transformation of the spin-echo signals. The spectral shape and position are almost the same, except for the slight further broadening of the spectra at low temperatures. This result indicates that the magnetic susceptibility is almost temperature-independent in the present material, which is consistent with the conventional Fermi-liquid picture.

These results show unambiguously that on an NMR timescale ($\sim\mu$s) there is no charge disproportionation. We shall argue that a dynamic disproportionation (that is, dynamic valence skipping with a timescale faster than $\sim\mu$s) that would amount to hopping of local electron pairs from site to site is also unlikely.

To this end, we have measured the temperature dependence of the ^{77}Se-NMR spin-lattice relaxation rate divided by the temperature $(T_1T)^{-1}$, as shown in Fig. 3. The ^{77}Se-NMR spin-lattice relaxation curves are well fitted by the single-exponential function, and thus the values of T_1 are well defined without serious distribution of the values. In case of dynamic pair hopping, we expect anomalous effects such as a pseudogap behavior due to preformed electron pairs [25,26] or a charge Kondo behavior [9–13]. Such anomalous behaviors

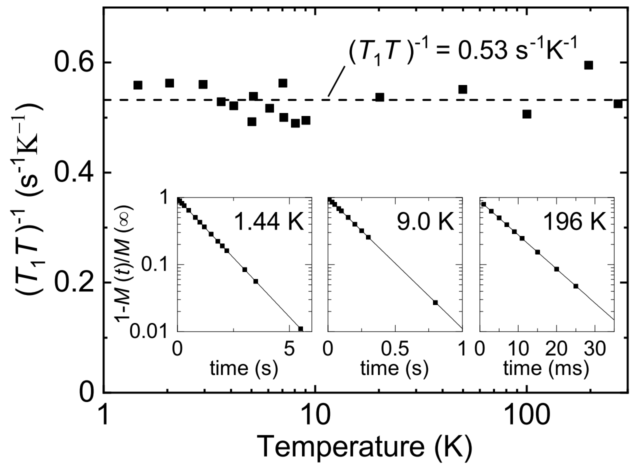

FIG. 3. Temperature dependence of $1/T_1T$ of the ^{77}Se-NMR signals of $AgSnSe_2$ under 8.7 T. The insets show the spin-lattice relaxation curves at several temperatures.

are characterized by deviations from the Korringa relation $(T_1T)^{-1}$ = const. However, ^{77}Se $(T_1T)^{-1}$ follows the Korringa relation very well, showing no anomalous behavior. We can conclude, therefore, that the electronic state of $AgSnSe_2$ is a conventional Fermi-liquid metal without a dynamical "valence skipping" effect.

V. THEORETICAL RESULTS

As opposed to other well-documented cases where similar calculations universally capture the valence skipping phenomenon [14,15,27–29], our crystal structure optimization did not reveal any charge disproportionation. Integrated charges within a Wigner-Seitz sphere around Sn show a single-peak distribution with about 0.05e width (Fig. 4). Calculating the bond valence sum around Sn (not shown) shows a similar one-mode distribution. This is consistent with the absence of static charge disproportionation deduced from our NMR data. Note that the number of about 12.1 valence electrons on Sn is not useful for the determination

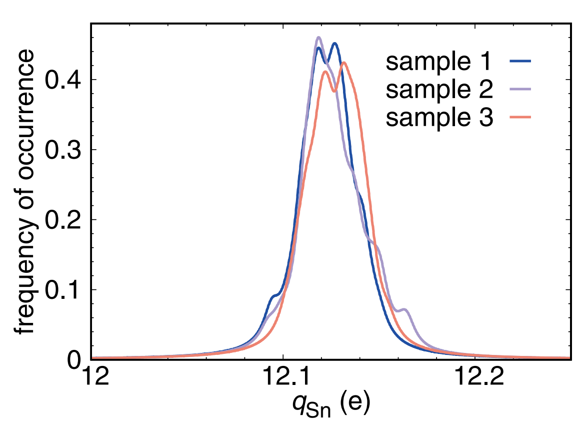

FIG. 4. Distribution of the calculated total valence charge on Sn in a 54-unit supercell with random disorder between Sn and Ag. Different colors correspond to different realizations of a random Ag–Sn distribution.

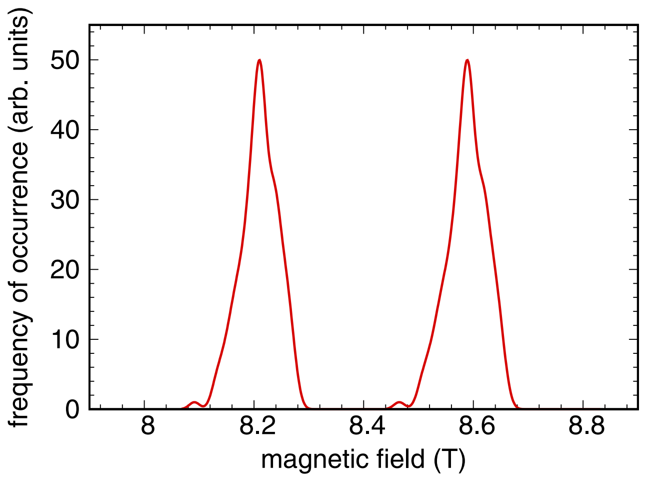

FIG. 5. Sn-NMR spectra as predicted by density functional calculations. No artificial broadening beyond that induced by statistical Ag–Sn disorder has been introduced.

of the valence and reflects incomplete integration of charge (PAW spheres leave a lot of interstitial). We have performed all-electron full potential local orbital [24] calculations to corroborate the PAW results. For the three realizations of disordered $AgSnSe_2$ shown in Fig. 4, we find for the 54 Sn ions in the supercell narrow charge distributions with less than $0.1e$ width centered at $49.36e$. We can compare this to the charges in typical materials with differentiated tin sites and nominal +2 and +4 charges. In Sn_2S_3 (*Pnma* space group) where Sn(1) and Sn(2) have distinct sulfur coordination and both XPS and NMR find indications for Sn(II) and Sn(IV) species [30], the calculation shows $48.93e$ on Sn(1) and $49.15e$ on Sn(2), *i.e.,* clearly different charges. In Sn_4P_3 ($R\bar{3}m$ space group) where Sn(1) and Sn(2) are in $SnSn_3P_3$ and SnP_6 coordination [31], respectively, the calculation shows $49.60e$ on Sn(1) and $49.36e$ on Sn(2). Thus, we can be sure that DFT calculations are reliable in showing the absence of charge disproportionation in $AgSnSe_2$.

Next, we have calculated the Knight shift on Sn using an ordered $AgSnSe_2$ cell with an alternating Ag and Sn layer ($P4/mmm$ space group). We found it to be completely dominated by the Fermi-contact term, reflecting the large density of s electrons at the Fermi level. The calculated Fermi-contact term is $2.40\% \pm 0.02\%$, while the core polarization is less than 0.02%, the anisotropic dipole term is less than 0.1% (the isotropic part is zero by symmetry), and the orbital term is -0.14% for the c direction and $+0.03\%$ for a/b. The directionally averaged orbital term is thus $\approx -0.08\%$ and the total shift $K \approx 2.32\%$, in excellent agreement with the experiment (2.3%–2.4%).

Since the Knight shift is nearly entirely decided by the Fermi-contact term, which is directly proportional to the partial s density of states N_s, we went back to our supercell calculations and plotted the distribution of N_s over all sites and three random realizations. In Fig. 5 we show the result. (In order to facilitate the comparison with the experiment in Fig. 1, we have taken the positions of the zero lines to match those in Fig. 1, namely, 8.404 and 8.792 T, and multiplied them by the calculated Knight shifts.) Not only the (anomalously large) widths but even the characteristic pseudotriangular shape is reproduced. This gives us confidence that the results are reliable, and no exotic physics beyond the standard density functional theory affects the electronic structure.

VI. CONCLUSIONS

We have investigated the electronic state of $AgSnSe_2$ experimentally by means of ^{119}Sn, ^{117}Sn, and ^{77}Se NMR spectroscopy and theoretically within the density functional theory. Both experiment and theory agree extremely well, and even though this compound is a natural candidate for valence skipping and negative-U superconductivity, they unambiguously indicate that neither static charge disproportionation nor dynamic electron pairing is realized in this compound. It appears to be a conventional Fermi-liquid metal where a very rare valence state of Sn^{3+} is realized.

ACKNOWLEDGMENT

We thank N. Hara and K. Fukuchi for experimental assistance in the NMR measurements. I.I.M. acknowledges support by ONR through the NRL basic research program and by the Research Institute for Interdisciplinary Science, Okayama University, visiting scientist program. This work was supported in part by JSPS KAKENHI Grant No. 18K03540.

[1] C. M. Varma, Missing Valence States, Diamagnetic Insulators, and Superconductors, Phys. Rev. Lett. **61**, 2713 (1988).

[2] J. E. Hirsch and D. J. Scalapino, Double-valence-fluctuating molecules and superconductivity, Phys. Rev. B **32**, 5639 (1985).

[3] H.-B. Schüttler, M. Jarrell, and D. J. Scalapino, Superconducting T_c Enhancement Due to Excitonic Negative-U Centers: A Monte Carlo Study, Phys. Rev. Lett. **58**, 1147 (1987).

[4] A. G. Mal'shukov, Superconductivity in metals containing negative-U centers, Exciton and phonon models, Solid State Commun. **77**, 57 (1991).

[5] S. H. Blanton, R. T. Collins, K. H. Kelleher, L. D. Rotter, and Z. Schlesinger, Infrared study of $Ba_{1-x}K_xBiO_3$ from charge-density-wave insulator to superconductor, Phys. Rev. B **47**, 996 (1993).

[6] C.-H. Du and P. D. Hatton, Observation of an incommensurate charge density wave in the oxide superconductor $Ba_{1-x}K_xBiO_3$, Europhys. Lett. **31**, 145 (1995).

[7] A. Yu. Ignatov, A. P. Menushenkov, K. V. Klementev, and D. I. Kochubey, Valency states of Bi in $BaPb_{1-x}Bi_xO_{3-\delta}$ and $Ba_{1-x}K_xBiO_{3-\delta}$ superconducting oxide, Nucl. Instrum. Methods Phys. Res., Sect. A **359**, 244 (1995).

[8] R. J. Cava, B. Batlogg, J. J. Krajewski, R. Farrow, L. W. Rupp, Jr., A. E. White, K. Short, W. F. Peck, and T. Kometani, Superconductivity near 30 K without copper: The $Ba_{0.6}K_{0.4}BiO_3$ perovskite, Nature (London) **332**, 814 (1988).

[9] Y. Matsushita, H. Bluhm, T. H. Geballe, and I. R. Fisher, Evidence for Charge Kondo Effect in Superconducting Tl-Doped PbTe, Phys. Rev. Lett. **94**, 157002 (2005).

[10] M. Matusiak, E. M. Tunnicliffe, J. R. Cooper, Y. Matsushita, and I. R. Fisher, Evidence for a charge Kondo effect in $Pb_{1-x}Tl_xTe$ from measurements of thermoelectric power, Phys. Rev. B **80**, 220403(R) (2009).

[11] T. A. Costi and V. Zlatić, Charge Kondo Anomalies in PbTe Doped with Tl Impurities, Phys. Rev. Lett. **108**, 036402 (2012).

[12] H. Matsuura and K. Miyake, Theory of charge kondo effect on pair hopping mechanism, J. Phys. Soc. Jpn. **81**, 113705 (2012).

[13] H. Mukuda, T. Matsumura, S. Maki, M. Yashima, Y. Kitaoka, K. Miyake, H. Murakami, P. Giraldo-Gallo, T. H. Geball, and I. R. Fisher, Anomalous ^{125}Te nuclear spin relaxation coincident with charge Kondo behavior in superconducting $Pb_{1-x}Tl_xTe$, J. Phys. Soc. Jpn. **87**, 023706 (2018).

[14] I. I. Mazin, D. I. Khomskii, R. Lengsdorf, J. A. Alonso, W. G. Marshall, R. M. Ibberson, A. Podlesnyak, M. J. Martínez-Lope, and M. M. Abd-Elmeguid, Charge Ordering as Alternative to Jahn-Teller Distortion, Phys. Rev. Lett. **98**, 176406 (2007).

[15] A. I. Liechtenstein, I. I. Mazin, C. O. Rodriguez, O. Jepsen, O. K. Andersen, M. Methfessel, Structural phase diagram and electron-phonon interactions in $Ba_{1-x}K_xBiO_3$, Phys. Rev. B **44**, 5388(R) (1991).

[16] L. Häggström, J. Gullmann, T. Ericsson, and R. Wäpplig, Mössbauer study of tin phosphides, J. Solid State Chem. **13**, 204 (1975).

[17] T. Wakita, E. Paris, K. Kobayashi, K. Terashima, M. Y. Hacisalihoğlu, T. Ueno, F. Bondino, E. Magnano, I. Píš, L. Olivi, J. Akimitsu, Y. Muraoka, T. Yokoya and N. L. Saini, The electronic structure of $Ag_{1-x}Sn_{1+x}Se_2$ ($x = 0.0$, 0.1, 0.2, 0.25 and 1.0), Phys. Chem. Chem. Phys. **19**, 26672 (2017).

[18] F. S. Nasredinov, S. A. Nemov, V. F. Masterov, and P. P. Seregin, Mössbauer studies of negative-U tin centers in lead chalcogenides, Phys. Solid State **41**, 1741 (1999).

[19] D. C. Johnston and H. Adrian, Superconducting and normal state properties of $Ag_{1-x}Sn_{1+x}Se_{2-y}$, J. Phys. Chem. Solids **38**, 355 (1977).

[20] Z. Ren, M. Kriener, A. A. Taskin, S. Sasaki, K. Segawa, and Y. Ando, Anomalous metallic state above the upper critical field of the conventional three-dimensional superconductor $AgSnSe_2$ with strong intrinsic disorder, Phys. Rev. B **87**, 064512 (2013).

[21] G. Kresse and J. Furthmüller, Efficient iterative schemes for ab initio total-energy calculations using a plane-wave basis set, Phys. Rev. B **54**, 11169 (1996).

[22] P. Blaha, K. Schwarz, G. K. H. Madsen, D. Kvasnicka, and J. Luitz, *Wien2k-05, An Augmented Plane Wave + Local Orbitals Program for Calculating Crystal Properties* (Karlheinz Schwarz, Techn. Universität Wien, Austria), ISBN 3-9501031-1-2.

[23] J. P. Perdew, K. Burke, and M. Ernzerhof, Generalized Gradient Approximation Made Simple, Phys. Rev. Lett. **77**, 3865 (1996).

[24] K. Koepernik and H. Eschrig, Full-potential nonorthogonal local-orbital minimum-basis band-structure scheme, Phys. Rev. B **59**, 1743 (1999).

[25] M. Randeria and E. Taylor, Crossover from Bardeen-Cooper-Schrieffer to Bose-Einstein condensation and the unitary Fermi gas, Annu. Rev. Condens. Matter Phys. **5**, 209 (2014).

[26] S. Kasahara, T. Yamashita, A. Shi, R. Kobayashi, Y. Shimoyama, T. Watashige, K. Ishida, T. Terashima, T. Wolf, F. Hardy, C. Meingast, H. v. Löhneysen, A. Levchenko, T. Shibauchi, and Y. Matsuda, Giant superconducting fluctuations in the compensated semimetal FeSe at the BCS-BEC crossover, Nat. Commun. **7**, 12843 (2016).

[27] E. Wawrzyńska, R. Coldea, E. M. Wheeler, I. I. Mazin, M. D. Johannes, T. Sörgel, M. Jansen, R. M. Ibberson, and P. G. Radaelli, Orbital Degeneracy Removed by Charge Order in Triangular Antiferromagnet $AgNiO_2$, Phys. Rev. Lett. **99**, 157204 (2007).

[28] I. Hase, T. Yanagisawa, and K. Kawashima, Electronic structure of SnF3: An example of valence skipper which forms charge density wave, Physica C **530**, 11 (2016).

[29] I. Hase, T. Yanagisawa, and K. Kawashima, One way to design a valence-skip compound, Nanoscale Res. Lett. **12**, 127 (2017).

[30] M. Cruz, J. Morales, J. P. Espinos, and J. Sanz, XRD, XPS and ^{119}Sn NMR study of tin sulfides obtained by using chemical vapor transport methods, J. Solid State Commun. **175**, 359 (2003).

[31] Y. B. Kuz'ma, S. I. Chikhrii, and V. N. Davydov, Refined crystal structure of Sn_4P_3, Inorg. Mater. **35**, 10 (1999)